PHYSICAL REVIEW B **77**, 020409(R) (2008)

Magnetovolume effect in $Mn_3Cu_{1-x}Ge_xN$ related to the magnetic structure: Neutron powder diffraction measurements

S. Iikubo,[1] K. Kodama,[1] K. Takenaka,[2,3] H. Takagi,[2,3] and S. Shamoto[1]
[1]*Quantum Beam Science Directorate, Japan Atomic Energy Agency, Tokai, Ibaraki, 319-1195, Japan*
[2]*RIKEN, The Institute of Physical and Chemical Research, Wako, Saitama 351-0198, Japan*
[3]*CREST, Japan Science and Technology Agency, Kawaguchi, Saitama 332-0012, Japan*
(Received 10 July 2007; revised manuscript received 3 December 2007; published 24 January 2008)

Magnetic structures in an antiperovskite system, $Mn_3Cu_{1-x}Ge_xN$, with a large magnetovolume effect above $x=0.15$ have been studied by neutron powder diffraction measurement. The present neutron study revealed that not only a cubic crystal structure but also a Γ^{5g} antiferromagnetic spin structure are key ingredients of the large magnetovolume effect in this itinerant electron system. The large magnetovolume effect is possibly ascribed to the geometrical frustration originating from the corner-shared octahedra of the antiperovskite structure.

DOI: 10.1103/PhysRevB.77.020409 PACS number(s): 75.80.+q, 61.05.fm, 65.40.De, 75.10.Lp

Negative thermal expansion (NTE) materials have already been used in a wide area of technical applications in which it is necessary to control the thermal expansion.[1,2] An important mechanism of NTE is the magnetovolume effect (MVE). With decreasing temperature (T), the volume can be expanded gradually by changing the amplitude of the magnetic moment. This MVE of itinerant electron systems has been investigated since the discovery of extraordinarily small thermal expansion in Invar alloys.[3] The MVE of Invar alloy systems is accompanied by other anomalous features in the elastic modulus, heat capacity, magnetization and Curie (or Néel) temperature, and has been an important problem closely connected to the origin of itinerant electron magnetism.[4–7]

Antiperovskite manganese nitrides Mn_3AN, where A is a metal or a semiconducting element, are well known for their large MVE.[8–11] The A atom occupies a cubic lattice corner position, whereas the Mn and N atoms locate at the face-centered and body-centered positions, respectively. These compounds have attracted much interest due to their variety of magnetic orderings and structural phase transitions.[8,12–16] Furthermore, much attention has been paid to the sharp first-order ferromagnetic phase transition, because of the potential for application in magnetic refrigeration technology.[17] So far, all the MVEs reported in Mn_3AN members are associated with first-order phase transitions. This is why Mn_3AN has not been considered as a practical NTE material to date, although the system has expanded volume at low temperature phase. Recently, Takenaka and Takagi reported that the MVE is broadened against T in $Mn_3Cu_{1-x}Ge_xN$ and leads to a giant negative thermal expansion coefficient.[18] This system shows three different characteristic behaviors of the MVE as a function of Ge concentration x. (i) Mn_3CuN shows the ferromagnetic transition at $T_C=143$ K accompanied by a cubic-to-tetragonal structural phase transition.[8] At the transition, the volume change is negligibly small. (ii) At $x=0.15$, the ferromagnetic transition takes place at $T_C\sim 100$ K and linear thermal expansion $\Delta L/L$ rapidly increases at that temperature with decreasing T. It must be noted that the T dependence of the magnetic susceptibility of $Mn_3Cu_{0.85}Ge_{0.15}N$ is qualitatively identical to that of Mn_3CuN. (iii) With increasing x, the magnetic transition temperature increases and the increase of $\Delta L/L$ occurs over a broader range of T. At $x\sim 0.5$, $\Delta L/L$ is almost linear to T in the temperature range of $270\leqslant T\leqslant 350$ K. The large negative coefficient of linear thermal expansion α is about -2×10^{-5}/K, one of the largest values among all NTE materials.

The MVE of itinerant electron systems has been discussed on the basis of the band picture, including spin fluctuation theory,[6] where local spin density plays an important role. The MVE in the Laves phase[4,5] is basically understood within this theoretical framework. Fruchart and Bertaut classified the magnetic properties of the Mn_3AN system on the basis of the band picture, similarly to the Hume-Rothery scheme.[8] They reported that the transition temperature of Mn_3AN is proportional to the number of valence electrons on A. On the other hand, there is no simple relationship between the magnitude of the MVE and the valence electron number. Therefore, we suggest that other effects are more relevant to the large MVE of this system. In this paper, in order to understand the Ge-doping effect on the magnetic properties and MVE in $Mn_3Cu_{1-x}Ge_xN$, we have studied the magnetic structure using neutron powder diffraction. The strong correlation revealed between large MVE and magnetic as well as crystal structures suggests a different paradigm.

Polycrystalline samples of $Mn_3Cu_{1-x}Ge_xN$ with $x=0$, 0.15, 0.2, and 0.5 were prepared by the solid-state reaction.[12,18–20] The experiments were performed on the high-resolution powder diffractometer HRPD ($\lambda=1.8233$ Å) and the triple axis spectrometer TAS-2 ($\lambda=2.3590$ Å) installed at JRR-3M of JAEA. Their collimations were open (effective value of 35′)-20′-6′ and 14′-40′-40′-80′, respectively. The powder samples of $Mn_3Cu_{1-x}Ge_xN$ weighing ~7 g were set in vanadium holders that were enclosed in Al cans filled with He gas. They were mounted in a closed-cycle refrigerator below room temperature and in a furnace above room temperature.

Figure 1 shows neutron diffraction patterns of (a) Mn_3CuN, (b) $Mn_3Cu_{0.85}Ge_{0.15}N$, and (c) $Mn_3Cu_{0.5}Ge_{0.5}N$. Solid lines show the data collected above and below magnetic ordering temperatures. Miller indices are given in reciprocal lattice units of primitive cubic perovskite with a lattice constant of ~3.90 Å. The diffraction pattern contains weak reflections, marked by stars, from MnO impurity and Al_2O_3 in the furnace. These peaks are removed in our analysis. Diffraction patterns of the three samples at high tempera-

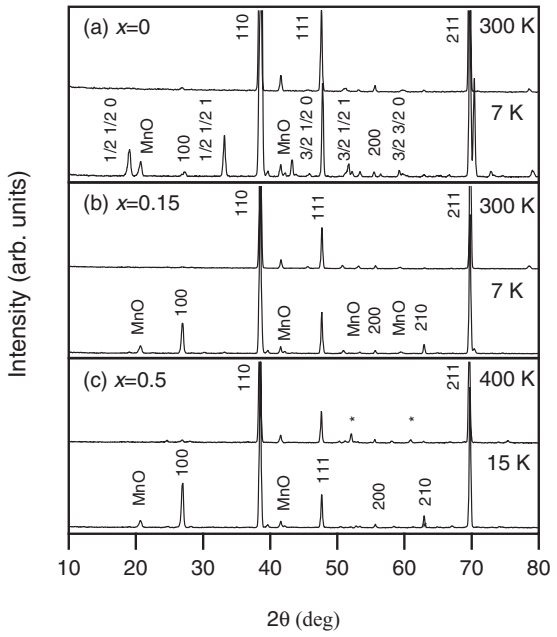

FIG. 1. Neutron powder diffraction patterns of (a) Mn_3CuN, (b) $Mn_3Cu_{0.85}Ge_{0.15}N$, and (c) $Mn_3Cu_{0.5}Ge_{0.5}N$ above and below magnetic ordering temperatures, which are at $T=300$ and 7 K for (a) and (b) and at $T=400$ and 15 K for (c), respectively.

tures are almost identical, indicating that all have the same primitive cubic unit cell. In Mn_3CuN, magnetic superlattice peaks with ordering vector $\boldsymbol{q}=(\frac{1}{2}\ \frac{1}{2}\ 0)$ appear at low temperatures, indicating that the magnetic unit cell becomes doubled along the a and b axes. Additionally, peak splitting is observed, for example, at the 2 1 1 reflection, because of the tetragonal distortion. These results are consistent with those in a previous report.[8] Detailed descriptions of the magnetic structure and its analysis are shown later. On the other hand, we cannot find any superlattice peaks or peak splitting in $Mn_3Cu_{0.85}Ge_{0.15}N$, $Mn_3Cu_{0.8}Ge_{0.2}N$, or $Mn_3Cu_{0.5}Ge_{0.5}N$ at low temperatures, indicating that both the crystal and magnetic structures have the same primitive perovskite unit cell, even at low temperatures. In Figs. 1(b) and 1(c), we can see similar magnetic reflections corresponding to magnetic ordering vector $\boldsymbol{q}=(0\ 0\ 0)$, where the 1 0 0 and the 2 1 0 magnetic reflection are strong.

The T dependence of the integrated intensities of these magnetic peaks is shown in Fig. 2(a), where the intensities are normalized by the 1 1 0 nuclear reflection intensity. These are mainly static magnetic reflections, but also contain small contributions from quasi-elastic magnetic scattering within the energy resolution ~1 meV. Figure 2(b) shows the T dependence of lattice constants estimated from the neutron diffraction study of $Mn_3Cu_{1-x}Ge_xN$ for $x=0$, 0.15, 0.2, and 0.5, which are consistent with the linear thermal expansions previously reported by Takenaka and Takagi.[18] The MVE at $x=0$ is negligible while the magnetic reflections show a rapid increase. Both the 1 0 0 magnetic reflection and the lattice constant exhibit sharp increases at $x=0.15$ and 0.2. For $x=0.5$, they gradually increase with decreasing T in the temperature range from 360 to 320 K.

The magnetic structure of Mn_3CuN, shown in Fig. 3(a),

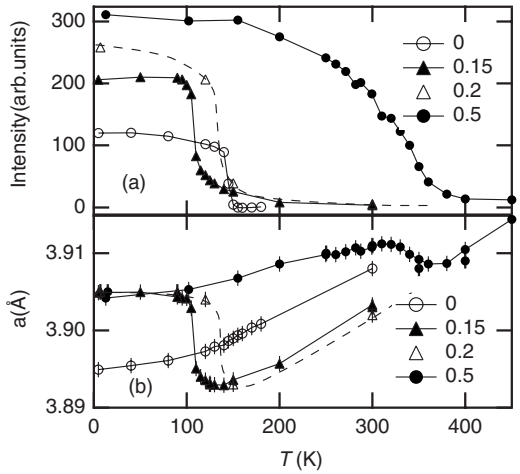

FIG. 2. (a) T dependence of magnetic peak intensity of $Mn_3Cu_{1-x}Ge_xN$. Open circles denote the $\frac{1}{2}\ \frac{1}{2}\ 0$ peak for $x=0$. Closed triangles, open triangles, and closed circles denote the 1 0 0 peak for $x=0.15$, 0.2, and 0.5, respectively. (b) T dependence of lattice constants of $Mn_3Cu_{1-x}Ge_xN$. At $x=0$, the average lattice constant is shown below the structural phase transition temperature (143 K).

has already been reported.[8] The Mn moments on the $z=0.5$ plane have a "square configuration" and a small ferromagnetic component along the c axis. The Mn moments on the $z=0$ plane have a parallel configuration. Ge-doped samples have a cubic structure (space group: $Pm\bar{3}m$) and magnetic ordering vector $\boldsymbol{q}=(0\ 0\ 0)$. On the basis of these conditions, three possible models have been proposed by Fruchart and Bertaut.[8] They considered a spin Hamiltonian with superexchange interactions among Mn ions up to the second nearest neighbors. The eigenstates consist of a collinear ferromagnetic structure and two triangular antiferromagnetic structures, where Mn moments point 120 degrees away from each other. The direction of Mn moments cannot be determined within the above consideration. The real spin structures are determined to be represented by the three models that are allowed by linear combination of the basis vectors of irreducible representations for the $Pm\bar{3}m$ group with $\boldsymbol{q}=(0\ 0\ 0)$. One is a ferromagnetic structure belonging to the irreducible representation Γ^{4g}, and two are antiferromagnetic (AF) structures belonging to Γ^{4g} and Γ^{5g}, respectively. For further details, refer to Bertaut and Fruchart.[21] Here, we can exclude the Γ^{4g} F structure, because the observed spontaneous magnetization for $x \geqslant 0.15$ is much smaller than the

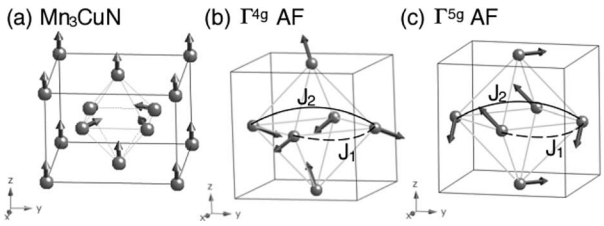

FIG. 3. (a) Magnetic structure of Mn_3CuN. (b) Γ^{4g} type antiferromagnetic cubic structure. (c) Γ^{5g} type antiferromagnetic cubic structure. Cu , Ge, and N atoms are omitted for simplicity.

TABLE I. Observed integrated intensities and total (nuclear+magnetic) intensities calculated using the model discussed in the text. Also included are the results calculated assuming the Γ^{4g} AF model for $x=0.5$.

	$x=0$			$x=0.15$		$x=0.5$		
hkl	I^{obs}	I^{cal}	*hkl*	I^{obs}	$I^{cal}_{\Gamma^{5g}}$	I^{obs}	$I^{cal}_{\Gamma^{5g}}$	$I^{cal}_{\Gamma^{4g}}$
$\frac{1}{2}\ \frac{1}{2}\ 0$	283(10)	341(0+341)	1 0 0	567(14)	561(25+535)	896(24)	890(29+861)	211(63+148)
1 0 0	50(5)	49(49+0)	1 1 0	2907(52)	2904(2701+204)	3036(75)	3061(2731+330)	3438(3162+276)
$\frac{1}{2}\ \frac{1}{2}\ 1$	320(7)	254(0+254)	1 1 1	577(15)	462(462+0)	516(10)	499(499+0)	556(556+0)
1 1 0	1000(21)	917(917+0)	2 0 0	46(2)	59(59+0)	47(2)	50(50+0)	42(42+0)
1 0 1	1752(25)	1809(1806+3)	2 1 0	130(3)	114(22+91)	175(4)	177(26+152)	138(51+86)
$\frac{2}{3}\ \frac{1}{2}\ 0$	105(4)	82(0+82)	2 1 1	1996(22)	2063(1979+84)	2222(11)	2200(2060+140)	2198(2160+38)
1 1 1	600(11)	599(595+4)	2 2 0	51(2)	66(66+0)	64(5)	58(58+0)	44(44+0)
$\frac{2}{3}\ \frac{1}{2}\ 1$	115(9)	105(0+105)	300/221	83(12)	46(17+28)	65(4)	69(21+49)	60(38+22)
2 0 0	0(0)	5(3+2)	3 1 0	1418(11)	1393(1380+13)	1568(26)	1502(1479+22)	1420(1405+15)
$\frac{3}{2}\ \frac{3}{2}\ 0$	29(2)	14(0+14)	3 1 1	650(12)	498(498+0)	557(8)	571(571+0)	522(522+0)
2 1 0	18(2)	47(47+0)	2 2 2	28(2)	36(36+0)	40 (3)	32(32+0)	22(22+0)
2 1 1	1450(10)	1422(1421+1)	2 3 0	14(5)	22(12+10)	27(3)	33(15+18)	29(25+4)

value expected from the ferromagnetic Γ^{4g} structure. Figures 3(b) and 3(c) show Γ^{4g} AF and Γ^{5g} AF magnetic structures. The ordering patterns imply that nearest-neighbor J_1 and next-nearest-neighbor J_2 are antiferromagnetic and ferromagnetic, respectively, and show the effect of the geometrical frustration originating from J_1. These two AF structures are energetically equivalent within the isotropic spin Hamiltonian, because all angles between Mn moments are 120 deg.

In this analysis, the total integrated intensities were analyzed because we found finite contributions of both the nuclear and magnetic reflections at several reciprocal lattice points. All atomic positions are fixed under the space group $P4/mmm$ for $x=0$ and $Pm\bar{3}m$ for $x\neq 0$. The amplitude of the magnetic moments was refined by the least-squares fitting program, where the isotropic magnetic form factor was used for Mn^{3+}.[22] The absorption and Lorentz factor corrections were made. Observed and calculated total (nuclear +magnetic) intensities are listed in Table I. For Mn_3CuN, the data were best fitted to the Fig. 3(a) model with $3.46\pm0.53\ \mu_B$ for the "square" component, where small ferromagnetic components at $z=0$ and $z=0.5$ were fixed to be 0.65 and 0.2 μ_B, as reported in Ref. 8. The average ferromagnetic moment, 0.35 μ_B, is consistent with the observed value in our magnetization measurements. The result is qualitatively consistent with that of Fruchart and Bertaut.[8] For Ge-doped samples at $x=0.15$ and 0.5, the data were fitted to both the Γ^{5g} AF and Γ^{4g} AF structures. $I^{cal}_{\Gamma^{5g}}$ can almost completely reproduce the observed intensities. The best fits were obtained with $2.02\pm0.16\ \mu_B$, $2.31\pm0.12\ \mu_B$, and $2.47\pm0.27\ \mu_B$ for $x=0.15$, 0.2, and 0.5, respectively. On the other hand, the Γ^{4g} AF structure cannot reproduce our data, as shown in $I^{cal}_{\Gamma^{4g}}$, which is the result of fitting $x=0.5$ data to the Γ^{4g} AF structure with $1.56\pm1.03\ \mu_B$. Large differences are observed at the 1 0 0 and 2 1 0 reflections, where magnetic intensities provide a large contribution. These results show that the systems with these x values have the Γ^{5g}-type antiferromagnetic structure shown in Fig. 3(c). The results were different from what we had expected. Because the T dependence of the magnetic susceptibility of $Mn_3Cu_{0.85}Ge_{0.15}N$ is qualitatively identical to that of Mn_3CuN,[18–20] $Mn_3Cu_{0.85}Ge_{0.15}N$ was expected to have cubic symmetry and the Mn_3CuN-type magnetic structure, as reported for Mn_3SnC.[8] Nevertheless, the present results clearly indicate that $Mn_3Cu_{0.85}Ge_{0.15}N$ has the same structure as $Mn_3Cu_{0.5}Ge_{0.5}N$. The ferromagnetic behavior of the susceptibility data at $x=0.15$ is due to the small canted ferromagnetic component.

Figure 4(a) shows the resulting T-x phase diagram of crystal and magnetic structures. In this figure, Curie and Néel temperatures estimated from magnetization measurements are plotted as open circles.[19] Magnetic transition temperatures determined by neutron diffraction studies are indicated by closed circles. It can be concluded that the MVE in $Mn_3Cu_{1-x}Ge_xN$ becomes significant in the Γ^{5g}-type antiferromagnetic cubic phase, while it is negligible in the tetragonal ferromagnetic phase. The MVE of an itinerant electron system has been discussed in terms of the amplitude of magnetic moment. However, the intimate relationship between the Γ^{5g} antiferromagnetic cubic structure and large MVE in $Mn_3Cu_{1-x}Ge_xN$ indicates the necessity of a theoretical

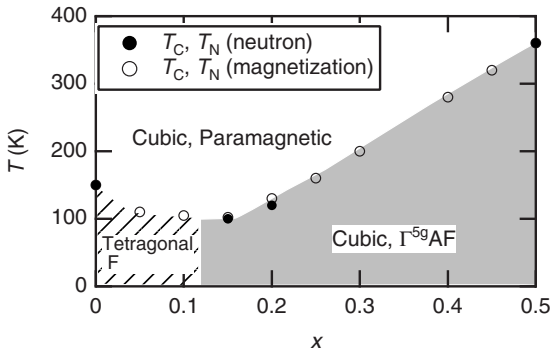

FIG. 4. (a) Phase diagram of $Mn_3Cu_{1-x}Ge_xN$. Open and closed circles denote Curie and Néel temperatures determined from magnetization measurements in Ref. 19 and neutron measurements, respectively. The MVE was observed in the hatched x range.

framework for MVE, in which the ordered magnetic structure is taken into account.

Let us now look at other antiperovskite materials. Mn_3GaN and Mn_3ZnN are well known for their large MVEs.[9,10] Their volumes show a sudden and pronounced increase with decreasing temperature at the first-order transition, and exhibit the Γ^{5g} antiferromagnetic structure in the cubic crystal structure below the phase transition temperature.[8] Furthermore, Mn_3ZnN undergoes another phase transition to a different magnetic structure at lower temperatures.[8] It is interesting to note that below the first-order transition, $\Delta L/L$ returns to the value expected from an extrapolation of the T dependence in the high-temperature phase.[10,18,23] Mn_3SnC has the cubic structure with the same spin arrangement as Mn_3CuN. The MVE of this compound is less pronounced than that in $Mn_3Cu_{1-x}Ge_xN$.[24] These results support the importance of the Γ^{5g} AF structure in producing a large MVE. Many antiperovskite materials with large MVEs have the cubic structure below T_N. The stability of the cubic structure reflects the characteristic electronic structure of these compounds, which prefer volume expansion to tetragonal distortion at the transition temperature.

The correlation between the large MVE and the cubic Γ^{5g} AF structure is possibly explained in terms of geometrical frustration. Corner-shared octahedra with AF nearest-neighbor interactions in a cubic antiperovskite structure are known to have three-dimensionally frustrated magnetic interactions,[25] which indeed lead the noncollinear spin structures in $Mn_3Cu_{1-x}Ge_xN$. When the frustration prevents the system from gaining magnetic energy because of short-range ordering above T_N, the system may earn kinetic energy by contracting its volume. This effect would enhance the MVE and/or the discontinuous change in $\Delta L/L$ at T_N. The high-temperature collinear ferromagnetic phase of Mn_3GaC, on the other hand, has much smaller MVE than that of $Mn_3Cu_{0.85}Ge_{0.15}N$,[9] suggesting that geometrical frustration might actually enhance the MVE in $Mn_3Cu_{0.85}Ge_{0.15}N$.

In summary, magnetic structures have been determined in $Mn_3Cu_{1-x}Ge_xN$. The system with the Γ^{5g} antiferromagnetic cubic structure, where the exchange interactions between the nearest-neighbor Mn moments are antiferromagnetic and lead to geometrical frustration, exhibits a large MVE in $Mn_3Cu_{1-x}Ge_xN$. The present results establish a MVE paradigm that will require a theoretical framework that takes into account the ordered magnetic structure.

We are grateful for useful discussions with K. Fukamichi, Y. Kakehashi, A. Fujita, and J. Matsuno. The authors thank N. Igawa and M. Matsuda for their help in the neutron diffraction measurements. This work was supported by a Grant-in-Aid for Scientific Research from the Ministry of Education, Culture, Sports, Science and Technology of Japan.

[1] A. W. Sleight, Inorg. Chem. **37**, 2854 (1998).
[2] A. W. Sleight, Curr. Opin. Solid State Mater. Sci. **3**, 128 (1998).
[3] C. E. Guillaume, Acad. Sci., Paris, C. R. **125**, 235 (1897).
[4] M. Shiga and Y. Nakamura, J. Phys. Soc. Jpn. **47**, 1446 (1979).
[5] R. Minakata, M. Shiga, and Y. Nakamura, J. Phys. Soc. Jpn. **41**, 1435 (1976).
[6] T. Moriya and K. Usami, Solid State Commun. **34**, 95 (1980).
[7] Y. Kakehashi, Physica B **161**, 143 (1989).
[8] D. Fruchart and E. F. Bertaut, J. Phys. Soc. Jpn. **44**, 781 (1978).
[9] Ph. l'Heritier, D. Boursier, R. Fruchart, and D. Fruchart, Mater. Res. Bull. **14**, 1203 (1979).
[10] R. Fruchart, R. Madar, M. Barberon, E. Fruchart, and M. G. Lorthioir, J. Phys. (Paris) **32**(C1), 982 (1971).
[11] D. Fruchart, E. F. Bertaut, R. Madar, G. Lorthioir, and R. Fruchart, Solid State Commun. **9**, 1793 (1971).
[12] T. Kaneko, T. Kanomata, and K. Shirakawa, J. Phys. Soc. Jpn. **56**, 4047 (1987).
[13] K. Motizuki and H. Nagai, J. Phys. C **21**, 5251 (1988).
[14] J. P. Bouchaud, Ann. Chim. (Paris) **3**, 81 (1968).
[15] K. Kamishima, T. Goto, H. Nakagawa, N. Miura, M. Ohashi, N. Mori, T. Sasaki, and T. Kanomata, Phys. Rev. B **63**, 024426 (2000).
[16] E. O. Chi, W. S. Kim, and N. H. Hur, Solid State Commun. **120**, 307 (2001).
[17] T. Tohei, H. Wada, and T. Kanomata, J. Appl. Phys. **94**, 1800 (2003).
[18] K. Takenaka and H. Takagi, Appl. Phys. Lett. **87**, 261902 (2005).
[19] K. Takenaka and H. Takagi, Mater. Trans. **47**, 471 (2006).
[20] K. Takenaka and H. Takagi, J. Jpn. Inst. Met. **70**, 764 (2006).
[21] E. F. Bertaut and D. Fruchart, Solid State Commun. **6**, 251 (1968).
[22] P. J. Brown, *International Tables for Crystallography*, edited by A. J. C. Wilson (Kluwer Academic, Dordrecht, 1992), Vol. C, Chap. 4.
[23] The appearance of the second phase transition in Mn_3ZnN depends on the sample preparation conditions. See Ref. 20 and W. S. Kim *et al.*, Phys. Rev. B **68**, 172402 (2003).
[24] Ph. l'Heritier, D. Boursier, and R. Fruchart, Mater. Res. Bull. **16**, 1511 (1981).
[25] D. Tahara, Y. Motome, and M. Imada, J. Phys. Soc. Jpn. **76**, 013708 (2007).